Inorganic Chemistry

Article

pubs.acs.org/IC

Homochiral Zinc(II) Coordination Compounds Based on In-Situ-Generated Chiral Amino Acid–Tetrazole Ligands: Circular Dichroism, Excitation Light-Induced Tunable Photoluminescence, and Energetic Performance

Shuai-Hua Wang,[†,‡] Fa-Kun Zheng,*[,†] Ming-Jian Zhang,[†,‡] Zhi-Fa Liu,[†,‡] Jun Chen,[†,‡] Yu Xiao,[†,‡] A-Qing Wu,[†] Guo-Cong Guo,[†] and Jin-Shun Huang[†]

[†]State Key Laboratory of Structural Chemistry, Fujian Institute of Research on the Structure of Matter, Chinese Academy of Sciences, Fuzhou, Fujian 350002, P. R. China

[‡]University of Chinese Academy of Sciences, Beijing 100039, P. R. China

Supporting Information

ABSTRACT: We employed two pairs of new in-situ-generated chiral amino acid–tetrazole ligands in constructing homochiral Zn(II) coordination compounds: $[Zn(tzet)]_n$ (**1a** for (*S*)-tzet and **1b** for (*R*)-tzet, H_2tzet = *N*-[2-(1*H*-tetrazol-5-yl)ethyl]tryptophan) and $[Zn(tzep)(H_2O)_2]\cdot H_2O$ (**2a** for (*S*)-tzep and **2b** for (*R*)-tzep, H_2tzep = *N*-[2-(1*H*-tetrazol-5-yl)ethyl]proline), which were hydrothermally synthesized and structurally characterized by single-crystal X-ray diffraction. Structural analysis reveals that **1** features a 2D homochiral framework generated by both tetrazolate and carboxylate bridges in $tzet^{2-}$ ligands. The isolated structure of **2** is stabilized by extensive hydrogen bonds, which leads to formation of a supramolecular 2D architecture. The absolute configuration induced at the nitrogen atoms of **1** and **2** is strictly related to the neighboring chiral carbon atoms by hydrogen-bond interactions. To further investigate their chirality, the combined experimental and theoretical analyses of circular dichroism spectra reveal the absolute configurations and nature of the Cotton effects. Solid-state excitation and emission spectra for **1** and **2** at room temperature were investigated with relevant density of states calculation, and tunable photoluminescence emission of **1** under different excitation wavelengths was discussed. As nitrogen-rich tetrazolate compounds, **1** and **2** possess higher enthalpies of combustion and may serve as a new family of promising energetic materials.

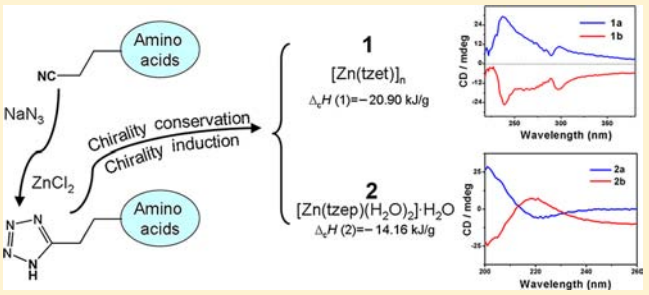

INTRODUCTION

In recent years, investigation of chiral coordination compounds (CCs) has been of particular interest due to their applications in chiral separation, asymmetric catalysis, enantioselective synthesis, and nonlinear optical materials.[1] However, obtaining homochiral CCs has been a challenging task in the pursuit of chiral and multifunctional materials.[2] Nowadays, three synthetic methods have usually been used to construct homochirality of CCs: (a) use of "induce" chiral auxiliaries, which induces spontaneous crystallization of only one enantiomorph.[3] (b) The most economical crystallization procedure is regarded as "spontaneous resolution" (but less predictable), in which molecules form condensates comprising only one enantiomer without a chiral resource. However, the spontaneous resolution of CCs from achiral components usually results in conglomerates through crystallization, an equal mixture with opposite chirality.[4] (c) The most convenient and reliable method to achieve bulk homochiral crystallization is "chirality conservation" by selecting enantiopure organic ligands, which impart homochirality to the frameworks of CCs.[5] Following this strategy, selection of chiral functional ligands becomes a key factor to obtain multifunctional chiral materials. Natural amino acids are known to construct CCs with chiral ligand naturally occurring in a chiral framework.[6] For example, L-proline chelates to the metal center in the N,O mode to form the homochiral CCs and inorganic–organic hybrid materials.[5a] Similarly, amino acid derivatives have also received significant attention.[7] However, amino acid–tetrazole compounds, simultaneously comprising amino acid and tetrazole groups, used in synthesizing homochiral CCs have rarely been studied.[8] Conversely, tetrazole-based compounds have exhibited increasingly special functionalities with interesting structures.[9] Combination of chiral amino acids and tetrazole groups can provide a feasible approach to build up diverse homochiral CCs with potential applications.

Herein, we chose *N*-terminal replaced chiral amino acids, *N*-(2-cyanoethyl)-proline (cet) and *N*-(2-cyanoethyl)-tryptophan

Received: June 4, 2013
Published: August 12, 2013

   dx.doi.org/10.1021/ic401409b | *Inorg. Chem.* 2013, 52, 10096–10104

(cep), as precursors to generate chiral amino acid−tetrazole ligands by in-situ [2 + 3] cycloaddition reaction of nitrile and azide.[10] We successfully obtained and structurally characterized two pairs of enantiomorphs, $[Zn(tzet)]_n$ (**1a** for (*S*)-tzet and **1b** for (*R*)-tzet, H_2tzet = *N*-[2-(1*H*-tetrazol-5-yl)ethyl]-tryptophan) and $[Zn(tzep)(H_2O)_2]\cdot H_2O$ (**2a** for (*S*)-tzep and **2b** for (*R*)-tzep, H_2tzep = *N*-[2-(1*H*-tetrazol-5-yl)ethyl]-proline) (Scheme 1). As expected, chirality conservation and chirality induction effects happened in the resultant compounds. The circular dichroism, photoluminescence emissions, and energetic performance of **1** and **2** have been experimentally and theoretically discussed.

Scheme 1. Syntheses of 1 and 2 with Marked Chiral Centers (*)

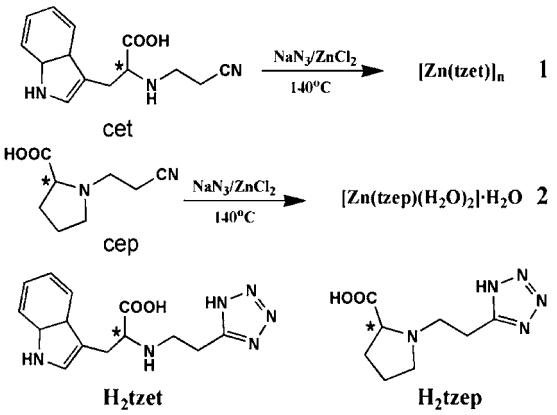

EXPERIMENTAL SECTION

Materials and Instruments. All reagents purchased commercially were used without further purification. Free ligands H_2tzet and H_2tzep were prepared by treating their respective coordination compounds with 1 N hydrochloric acid according to our previously described procedure.[11] Powdered X-ray diffraction (PXRD) patterns were collected on a Rigaku Miniflex II diffractometer using Cu Kα radiation (λ = 1.540598 Å) at 40 kV and 40 mA in the range of $5° \leq 2\theta \leq 80°$. Simulated PXRD patterns were derived from the Mercury Version 1.4 software (http://www.ccdc.cam.ac.uk/products/mercury/). Elemental analyses were performed on an Elementar Vario EL III microanalyzer. FT-IR spectra were obtained on a Perkin-Elmer Spectrum using KBr disks in the range 4000−400 cm^{-1}. Thermogravimetric analysis (TGA) experiments were done on an NETZSCH STA 449C Jupiter thermogravimetric analyzer in N_2 with the sample heated in an Al_2O_3 crucible at a heating rate of 10 K min^{-1}. Determination of photoluminescence (PL) and lifetime was conducted on a double-excitation monochromator Edinburgh FL920 fluorescence spectrometer equipped with a R928 PMT detector. Solid-state circular dichroism (CD) spectra were performed on a Bio-Logic MOS-450 CD spectrometer (France) in a KCl matrix at 25 °C. Combustion heats were measured by oxygen bomb calorimetry (5E-AC8018, Changsha Kaiyuan Instruments Co., Ltd., China).

Syntheses of 1 and 2. All new compounds were prepared following a similar procedure. The reaction mixture of NaN_3 (0.5 mmol), $ZnCl_2$ (0.5 mmol), and (*S*)-cet/(*R*)-cet/(*S*)-cep/(*R*)-cep (0.5 mmol) in 8.0 mL of distilled water was sealed into a 25 mL Teflon-lined stainless steel vessel under autogenous pressure and then heated to 140 °C in 2 h, kept to this temperature for 2 days, and cooled to room temperature at a rate of 5 °C/h. Prismatic or block crystals suitable for X-ray analysis were obtained. Yield: 25% (based on Zn) for **1a**; 28% (based on Zn) for **1b**; 61% (based on Zn) for **2a**; 55% (based on Zn) for **2b**. Anal. Calcd for $C_{14}H_{14}N_6O_2Zn$ (**1a**): C, 46.23; H, 3.88; N, 23.11. Found: C, 45.69; H, 3.86; N, 22.93. Anal. Calcd for $C_{14}H_{14}N_6O_2Zn$ (**1b**): C, 46.23; H, 3.88; N, 23.11. Found: C, 45.89; H, 3.80; N, 23.06. Anal. Calcd for $C_8H_{17}N_5O_5Zn$ (**2a**): C, 29.24; H, 5.21;

Table 1. Pertinent Crystal Data and Structure Refinement Results for 1 and 2

	1a	1b	2a	2b
formula	$C_{14}H_{14}N_6O_2Zn$	$C_{14}H_{14}N_6O_2Zn$	$C_8H_{17}N_5O_5Zn$	$C_8H_{17}N_5O_5Zn$
M_r (g mol^{-1})	363.68	363.68	328.64	328.64
size (mm)	0.32 × 0.18 × 0.16	0.28 × 0.13 × 0.11	0.25 × 0.25 × 0.21	0.28 × 0.26 × 0.12
cryst shape	prism	prism	block	block
cryst syst	orthorhombic	orthorhombic	monoclinic	monoclinic
space group	$P2_12_12_1$	$P2_12_12_1$	*C*2	*C*2
a (Å)	7.125(4)	7.107(2)	22.757(5)	22.911(2)
b (Å)	8.357(5)	8.357(3)	7.699(2)	7.7031(6)
c (Å)	26.60(2)	26.572(9)	7.263(2)	7.3610(7)
β (deg)	90	90	90.948(3)	90.668(6)
V (Å^3)	1584(2)	1578.1(9)	1272.2(5)	1299.0(2)
Z	4	4	4	4
d_c (g cm^{-3})	1.525	1.531	1.716	1.680
T (K)	293(2)	293(2)	293(2)	293(2)
F(000)	744	744	680	680
no. of reflns	10 735	12 430	2836	2359
R_{int}	0.0553	0.0506	0.0167	0.0229
params	208	208	190	190
S on F^2	1.078	0.982	1.015	1.007
R_1 ($I > 2\sigma(I)$)	0.0418	0.0409	0.0186	0.0228
wR_2 ($I > 2\sigma(I)$)	0.0733	0.0783	0.0396	0.0413
R_1 (all data)	0.0527	0.0526	0.0199	0.0261
wR_2 (all data)	0.0783	0.0833	0.0399	0.0421
ρ_{max}/ρ_{min} (e Å $^{-3}$)	0.394/−0.464	0.371/−0.287	0.267/−0.250	0.177/−0.176
Flack	0.03(2)	0.036(17)	0.035(8)	0.047(10)
CCDC	939938	939939	939940	939941

dx.doi.org/10.1021/ic401409b | *Inorg. Chem.* 2013, 52, 10096−10104

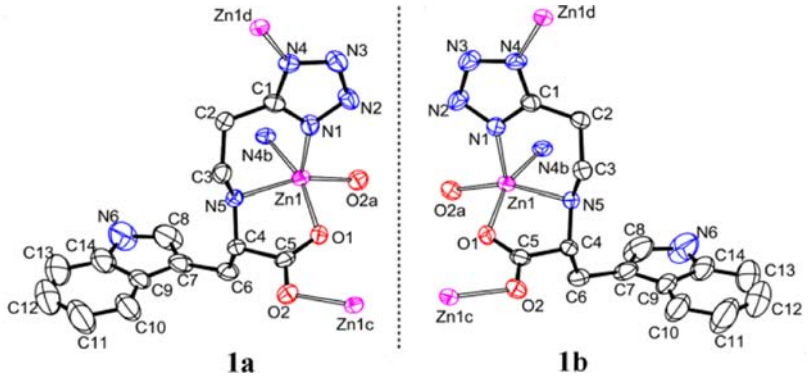

Figure 1. Two mirror images of coordination environments of **1a** and **1b**. Symmetry codes: (a) $x + 1/2, -y + 3/2, -z$; (b) $x + 1/2, -y + 5/2, -z$; (c) $x - 1/2, -y + 3/2, -z$; (d) $x - 1/2, -y + 5/2, -z$.

N, 21.31. Found: C, 29.12; H, 5.12; N, 21.26. Anal. Calcd for $C_8H_{17}N_5O_5Zn$ (**2b**): C, 29.24; H, 5.21; N, 21.31. Found: C, 29.25; H, 5.10; N, 21.34. IR (KBr pellet, cm^{-1}) for **1a**: 3411m, 3252m, 2912w, 1620vs, 1583vs, 1456s, 1420s, 1336m, 1227m, 1096s, 994s, 933m, 741s, 617w, 581w. IR (KBr pellet, cm^{-1}) for **1b**: 3411m, 3235m, 2906w, 1618vs, 1586vs, 1452s, 1412s, 1337m, 1218m, 1088s, 997s, 936m, 747s, 615w, 585s. IR (KBr pellet, cm^{-1}) for **2a**: 3301s, 2975s, 2256w, 1633vs, 1497m, 1464w, 1419s, 1366vs, 1337m, 1310m, 1130m, 1096m, 1062m, 978w, 941w, 715m. IR (KBr pellet, cm^{-1}) for **2b**: 3265s, 2972s, 2300w, 1636vs, 1497m, 1416s, 1366vs, 1309m, 1131m, 1093m, 975w, 938w, 716m.

Crystal Structure Determination. Single-crystal X-ray diffraction measurements were carried out on a Rigaku Mercury CCD diffractometer, which was equipped with Mo Kα radiation (λ = 0.71073 Å), using the ω-scan technique for collection of the intensity data sets and corrected for Lp effects. Primitive structures were solved by direct methods and reduced by the CrystalClear software.[12] Subsequent successive difference Fourier syntheses yielded the other non-hydrogen atoms. Hydrogen atoms of ligands were added geometrically and refined using the riding model. Hydrogen atoms of all water molecules were located in the idealized positions and refined with O−H distances restrained to a target value of 0.85 Å, the H···H distance to 1.34 Å, and $U_{iso}(H) = 1.5U_{eq}(O)$. Final structures were refined using a full-matrix least-squares refinement on F^2. All of the calculations were performed by the Siemens SHELXTL version 5 package of crystallographic software.[13] Pertinent crystal data and structural refinement results and selected bond distances and angles for **1** and **2** are listed in Tables 1 and S1, Supporting Information, respectively.

Calculation of the Density of States (DOS). X-ray crystallographic data for **1a** and **2a** were used to calculate the density of states (DOS). Calculation of the DOS was carried out with density functional theory (DFT) with one of the three nonlocal gradient-corrected exchange-correlation functionals (GGA-PBE), and performed with the CASTEP code in the Materials Studio v4.0 software package,[14] which uses a plane wave basis set with Vanderbilt ultrasoft pseudopotentials for the core electrons. The number of plane waves included in the basis was determined by a cutoff energy of 340.0 eV for **1a** and **2a**, and numerical intergration of the Brillouin zone was performed with a 1 × 1 × 1 Monkhorst−Pack k-point sampling for accurate calculation of the optical properties of the compounds. Other parameters in the calculations were set to the CASTEP code default values.

RESULTS AND DISCUSSION

Synthesis. Enantipure 5-substituted tetrazoles were prepared by in-situ [2 + 3] cycloaddition reaction of nitrile and azide in the presence of Lewis acids (Zn salts) by the hydrothermal method.[10] The synthetic route of homochiral CCs **1** and **2** is illustrated in Scheme 1. In our lab, a series of cyano compounds has been employed to synthesize tetrazole-based CCs, and we found that the value of pH plays a dominant role in governing [2 + 3] cycloaddition reaction of cyano and azide, such as slightly alkaline suitable for 3-cyano propionate.[15] However, it is favorable for 2-cyanoethyl amino acids to react with azide only under acidic conditions. The occurrence of the cycloaddition reaction was evidenced by the IR spectra, where the diagnostic peak of the cyano group around 2100 cm^{-1} disappeared and the peaks of the tetrazolate group (at ca. 1464 and 1419 cm^{-1} for **1a**, at ca. 1497 and 1416 cm^{-1} for **1b**, at ca. 1456 and 1420 cm^{-1} for **2a**, at ca. 1452 and 1412 cm^{-1} for **2b**) emerged (Figure S1, Supporting Information). The experimental PXRD patterns of bulky products are in good agreement with the calculated ones based on the single-crystal structures, indicating a pure phase of **1** and **2** (Figure S2, Supporting Information). Thermogravimetric analyses (TGA) experiments for **1** and **2** were tested in N_2 atmosphere in the temperature range of 30−800 °C (Figure S3, Supporting Information). The TGA curve of **1** began to vary until up to 380 °C, which may be the consequence of no coordinated or lattice water molecules and indicates the crystal structure of **1** is thermally stable. Compound **2** has a weight loss of 15.3% up to 140 °C in accordance with release of three lattice water molecules (calcd 16.4%), and no weight loss occurred until heating up to approximate 320 °C. The thermal stabilities of **1** and **2** are further confirmed by variable-temperature PXRD patterns (Figure S4, Supporting Information). As the temperature increased to 400 °C, the molecular framework of **1** remained stable, and continuous heating led to framework collapse, presumably due to decomposition of organic ligand. The molecular framework of **2** can only be thermally stable up to 100 °C, and successive heating may result in formation of the unknown amorphous compound.

Structural Descriptions and Discussions. *1a* and *1b*. Compounds **1a** and **1b** are a pair of enantiomorphs, and both crystallize in the $P2_12_12_1$ space group. Taking compound **1b** for example, each asymmetric unit comprises one Zn(II) atom and one $tzet^{2-}$ ligand (Figure 1). The $tzet^{2-}$ ligand chelates the Zn(II) center through the N1, N5, and O1 positions to form a five/six-membered ring structure mainly due to the shorter alkyl spacer. The Zn(II) atom has a tetragonal pyramid geometry ($\tau = 0.03$)[16] with the equatorial plane formed by two N and two O atoms from three different $tzet^{2-}$ ligands with rational bond lengths from 1.986(2) to 2.143(2) Å and the apical position occupied by N1 atom. Each $tzet^{2-}$ ligand is coordinated to three Zn(II) ions through carboxylate oxygen atoms (O1 and O2) and tetrazolate nitrogen atoms (N1 and N4), which can be regarded as a triply bridging ligand. The

dx.doi.org/10.1021/ic401409b | Inorg. Chem. 2013, 52, 10096−10104

carboxylate group bridges two Zn(II) atoms in the syn−anti configuration to form a helical chain with a Zn···Zn distance of 4.960(1) Å along the *a* axis. Adjacent chains are connected by μ_2-κN1:κN4 bridging tetrazolate rings to generate a 2D layer network parallel to the *ab* plane (Figure 2a), where the indole

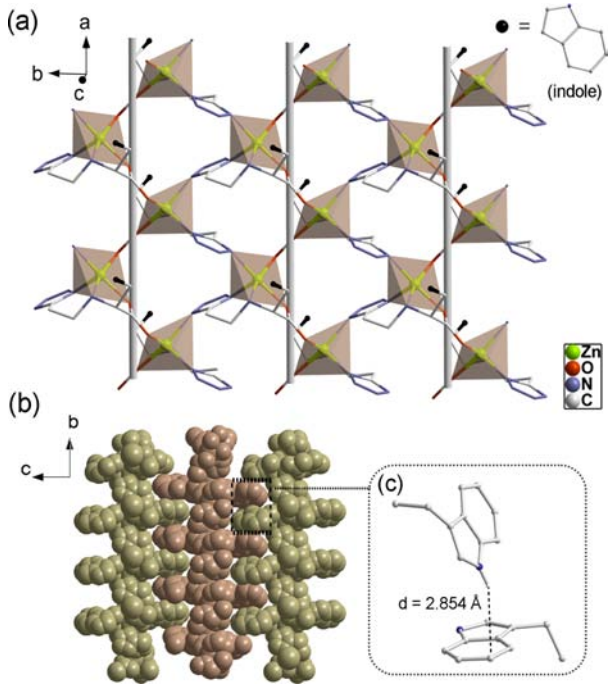

Figure 2. (a) Structure of 2D network in **1b**; (inset) simplified indole group. (b) −ABAB− layered arrangement of **1b** along the *c* axis. (c) N−H···π interactions between two adjacent indole rings.

rings are regularly located in two opposite sides of the layer. The 2D layers are stacked in an −ABAB− sequence along the *c* direction with an interlayer distance of 13.286(2) Å (Figure 2b). The π-stacking interactions exist between adjacent layers, which would be better described as N−H···π attractions, with a 2.854 Å distance of H6N to the neighboring indole ring (Figure 2c).[17]

2a and 2b. Similar to compounds **1a** and **1b**, a pair of enantiomorph **2a** and **2b** both crystallize in the *C*2 space group with **2b** as a representative for detailed structural discussions. There exists one Zn(II) atom, one $tzep^{2-}$ ligand, two coordinated water molecules, and one lattice water molecule in an asymmetric unit (Figure 3). The Zn(II) atom is five coordinated by one O atom and two N atoms from one $tzep^{2-}$ ligand and two O atoms from water molecules to furnish a distorted trigonal bipyamidal geometry (τ = 0.70) with the O/N−Zn−O/N angles varying from 80.14(7)° to 128.11(8)°. The O1W atom of the coordinated water molecule and tertiary amine N5 atom are located at the axial positions with bond lengths of 2.121(2) and 2.209(2) Å, respectively. Like the $tzet^{2-}$ ligand, $tzep^{2-}$ is bound to the Zn(II) atom through the N1, N5, and O1 positions to form a five/six-membered ring structure, which leads to formation of an isolated mononuclear Zn(II) compound **2b**. Interestingly, structural examination shows that a variety of strong intermolecular hydrogen bonds exist. Hydrogen bonds between the coordinated water O1W and carbonyl group O1═C8 from the adjacent molecule result in formation of a dimeric unit (O1W−H1WB···O1#1 and O1W#1−H1WB#1···O1, #1: 1 − *x*, *y*, 1 − *z*). Adjacent dimers

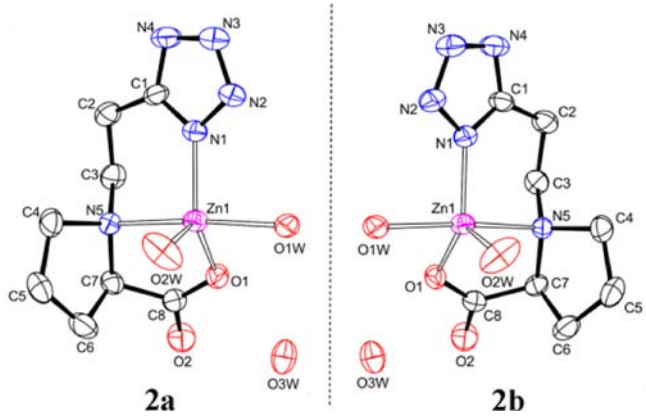

Figure 3. Enantiomeric coordination environments of **2a** and **2b**.

are interconnected by two O2W−H2WB···O1W hydrogen bonds to form 1D chains along the *c* axis. The lattice water O3W molecules are found to exist in three-bridging H-bond interactions with O2, O2W, and N3 atoms, involved with hydrogen bonds of O3W−H3WA···O2, O2W−H2WA···O3W, and O3W−H2WB···N3. With respect to the relative orientations of the tetrazole groups, the interweave of neighboring chains by the three-bridging O3W atoms and hydrogen bonds of O1W−H1WA···N4 produces a supramolecular 2D layered framework parallel to the *bc* plane (Figure 4). The adjacent layers are stacked in an −ABAB− sequence along the *a* direction (Figure S5, Supporting Information). The structure of **2b** is stabilized by strong hydrogen bonds with the related parameters listed in Table S2, Supporting Information.

On the basis of the above-mentioned structural analysis, the ligands with the definite chiral center are prone to obtain homochiral CCs. The chiral center of the ligand can be shifted into the framework of CCs with maintenance of configuration, named "chirality conservation". However, secondary/tertiary amine ligands produce a new chiral N center with two kinds of orientations when the N atom coordinates to metal atoms. It is an inevitable challenge with uncertain chirality to get optically pure materials.[18] In our previous work, we selected a secondary amine compound (*N*-[2-(1*H*-tetrazol-5-yl)ethyl]-glycine) for constructing tetrazolate compounds and found that a chiral *N* center was generated in the CCs with *R* and *S* chirality coexistence.[19] Interestingly, in this study, we successfully built up four homochiral CCs including single chiral N centers. As secondary amine $tzet^{2-}$ ligands in **1**, N1 and N5 atoms chelate to the Zn1 atom to form a stable six-membered ring containing N1, C1, C2, C3, N5, and Zn atoms. In addition, the carboxylate group and tetrazolate group of another $tzet^{2-}$ ligand lie in two opposite sides of the six-membered ring (Figure S6, Supporting Information). The hydrogen-bond interaction (N5−H5N···N3b) stabilizes the H5N atom located in an opposite side to the carboxylate group and finally induces single chirality of the N5 atom ((*S*)-C4 and (*R*)-N5 for **1a**, (*R*)-C4 and (*S*)-N5 for **1b**). For tertiary amine $tzep^{2-}$ ligand, the chelation action and ring intention prompt formation of C7 chiral configuration to induce a solely chiral N5 orientation ((*S*)-C7 and (*R*)-N5 for **2a**, (*R*)-C7 and (*S*)-N5 for **2b**), where the hydrogen bond also plays an important role in fixing the configuration of N5 atoms.[20] Certainly, coordination fashions of amino acid−tetrazole ligands have great effects on the molecular architecture of the formed CCs. The $tzet^{2-}$ ligand in **1** behaves

dx.doi.org/10.1021/ic401409b | *Inorg. Chem.* 2013, 52, 10096−10104

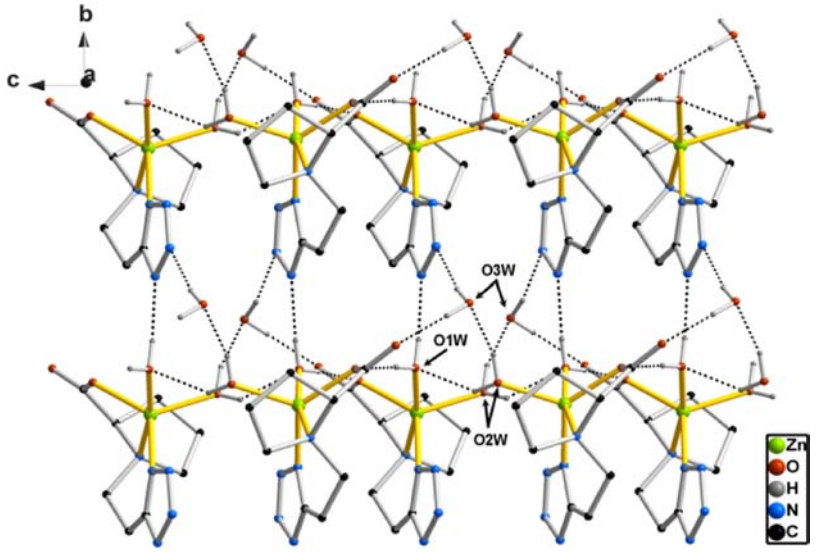

Figure 4. Supramolecular 2D sheets formed by hydrogen bonds in **2b**.

in a μ_3-κO1,N1,N5:κO2:κN4 mode beneficial for construction of a 2D network, while the $tzep^{2-}$ ligand in mononuclear **2** merely exhibits a tridentate chelation style.

Circular Dichroism Properties. Circular dichroism (CD) spectroscopy, based on the differential absorption of right and left circularly polarized light, plays an important role in studying chiral compounds and analyzing their geometric structures. The absolute configuration of homochiral CCs can also be confirmed by the positive or negative CD signals. Moreover, theoretical advances in quantum chemical calculation methods allow us to investigate CD intrinsic mechanism.[21] The calculated transition energy (eV), oscillator *f*, rotational strength *R*, and contributions of **1a** and **2b** are listed in Table S3, Supporting Information. A Gaussian function is commonly used as the broadening function for CD spectra with the width of the band (σ), excitation energies (ΔE_i), and rotatory strengths (R_i) as follows

$$\Delta\varepsilon(E) = \frac{1}{2.297 \times 10^{-39}} \frac{1}{\sqrt{2\pi\sigma}} \sum_{i}^{A} \Delta E_i R_i e^{[-(E-\Delta E_i/2\sigma)]^2}$$

Solid-state CD spectra of **1a** and **1b** (Figure 5a) denote two positive Cotton effects at λ = ~297 and ~237 nm for **1a** (two negative ones for **1b**) and the enantiomeric nature of **1a** and **1b**. To elucidate the predominant mechanism of the solid-state CD spectra, additional calculations have been performed using Gauss software.[22] The dinuclear molecular fragment ($[Zn_2(tzet)_2]$) of **1a** was selected to calculate at the TDHF/6-31G** level, which was generated by the SpecDis software.[23] The calculated CD and UV spectra of **1a** are displayed with the simulated ones red shifted by 50 nm for a convenient comparison between the theoretical and the experimental results (Figure 5b and Figure S7, Supporting Information). The molecular orbitals (MOs) of **1a** involved with the main transitions are illustrated in Figure 5c. On the basis of the calculated CD spectra, the first positive Cotton effect (at ~297 nm) is mainly attributed to the transition from states 8 to 12. State 8 includes the orbitals from 169 to 187 (+59%), which reveals a partial contribution originating from LMCT interactions from the carboxylate groups to the Zn^{2+} atoms. By analysis of transition states 9−12, the calculated results show that the π−π* transition of the indole group is the main

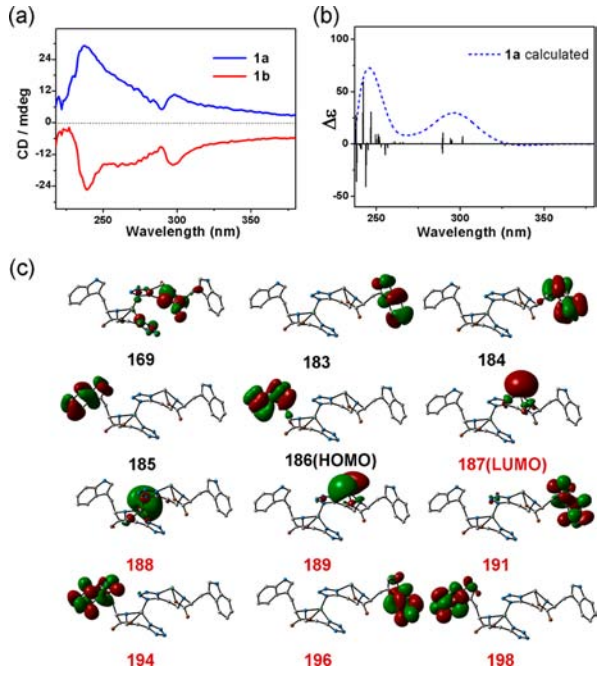

Figure 5. (a) Experimental CD spectra of **1a** (blue) and **1b** (red). (b) Theoretical CD spectrum of **1a** red shifted by 50 nm for a convenient comparison with bar representation of the rotatory strength. (c) Molecular orbitals associated with the main transitions. Labels for the occupied and virtual orbitals are indicated in black and red, respectively.

contribution for the positive Cotton effect at ~297 nm (186−194 (+70%), 184−191 (+66%), 183−191 (+63%), and 185−194 (+66%), respectively). The other positive Cotton effect (at ~237 nm) should be ascribed to states 30, 35, 40, and 42. For state 30, the transition from orbitals 184−189 demonstrates the LMCT interaction from indole groups to Zn(II) atoms. The transitions of the states (35, 40, and 42) mainly contain 186−198 (+40%), 185−198 (+49%), and 183−196 (+44%), respectively, which reveals that energy transitions mainly come from internal conjugated systems of indole groups. In view of the forementioned discussions, the chromophores of indole groups make major contributions to the Cotton effects

dx.doi.org/10.1021/ic401409b | *Inorg. Chem.* 2013, 52, 10096−10104

of **1a**, which can also be testified by the solid CD spectra of free (*S*)/(*R*)-H_2tzet ligands. There are two positive Cotton effects at λ = ~310 and ~260 nm for (*S*)-H_2tzet (two negative ones for (*R*)-H_2tzet) (Figure S8a, Supporting Information).

As shown in Figure 6a, **2a** exhibits a positive Cotton effect at ~205 nm and a negative Cotton effect at ~220 nm while **2b**

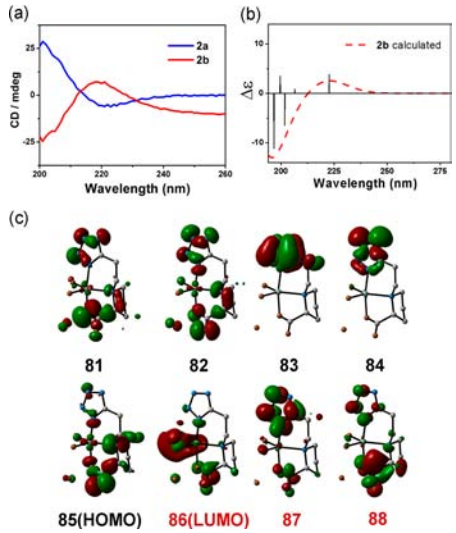

Figure 6. (a) Experimental CD spectra of **2a** (blue) and **2b** (red). (b) Theoretical CD spectrum of **2b** with bar representation of the rotatory strength. (c) Molecular orbitals associated with the main transitions. Labels for the occupied and virtual orbitals are indicated in black and red, respectively.

shows opposite Cotton effects to **2a**. CD spectra of **2a** and **2b** are nearly mirror-symmetric images, which indicates the expected formation of a pair of enantiomeric compounds. Additional calculations have been performed using time-dependent density functional theory (TD-DFT) employing the B3LYP functional, including polarization and diffuse functions (6-31G**) (Table S3, Supporting Information).[24] The calculated CD spectrum of **2b** is in good agreement with the experimental one (Figure 6b). Obviously, the positive Cotton effect at ~220 nm (state 1) for **2b** is mainly attributed to the transitions from orbitals 85 to 88 (+45%) and 85 to 86 (+27%), which is mainly due to the n−π* transition of the carboxylate groups and LMCT interactions from the N5 atoms to Zn(II) atoms. States 5 and 6 should arouse a negative Cotton effect for **2b** at ~205 nm, containing electronic transitions from orbitals 81 to 88, 81 to 86, 84 to 86, and 83 to 86. The main contributions to this band come from the carboxylate n−π* transition and LMCT interactions from the tetrazolate groups to Zn(II) atoms.[25] By comparing the CD spectra of free ligand H_2tzep (Figure S8b, Supporting Information) and its coordination compound **2b**, an additional positive Cotton effect at ~220 nm in **2b** emerged due to LMCT interactions.

Luminescent Properties. The solid-state excitation and emission spectra for **1a** were investigated at room temperature (Figure 7a), and **1a** displays a maximum emission of 320 nm under the 300 nm excitation wavelength. The emission peak of **1a** lies in near-ultraviolet region; however, the emission exhibits dark-blue fluorescence to the naked eyes, which implies that visible emissions and multiple emitting centers exist. Notably, when excited at >300 nm, the emission of 320 nm disappears. When excited from 310 to 350 nm, the emission peaks locate in the range of 350−390 nm, where **1a** shows a strong blue fluorescence (Figure 7b). When excited from 360 to 380 nm, the emission peak moves to the scope of 430−470 nm and **1a** shows a light blue fluorescence (Figure 7c). Thus, **1a** exhibits tunable UV-to-blue photoluminescence upon variation of excitation wavelengths. The luminescence lifetime measurements show that the values of the fluorescent lifetime are 1.46 (τ_1 = 1.37 ns, 95.69%; τ_2 = 3.45 ns, 4.31%) and 3.57 ns (τ_1 = 2.09 ns, 83.18%; τ_2 = 5.13 ns, 9.23%; τ_3 = 17.87 ns, 7.58%) for 320 and 430 nm emissions (Figure S9, Supporting Information), which are indicative of fluorescence of indole and tetrazolate groups, respectively. To understand better the photoluminescent mechanism, the density of states (DOS) are theoretically calculated (Figure S10, Supporting Information). The results indicate that the top of the valence bands (VBs) of **1a** is dominated by indole groups, while the bottom of the conduction bands (CBs) is mainly contributed by the mixture of indole and tetrazolate groups. On the whole, Zn(II) atoms make no or less contribution to the top of the VBs or the bottom of the CBs. Theoretically speaking, when excited at 300 nm, intraligand-centered transitions (ILCT) of indole groups play a main role with an emission of 320 nm.[26] When excited at 310−350 nm, the mixed ILCT of indole and tetrazolate groups coexist (Figure S11a, Supporting Information). With excitation

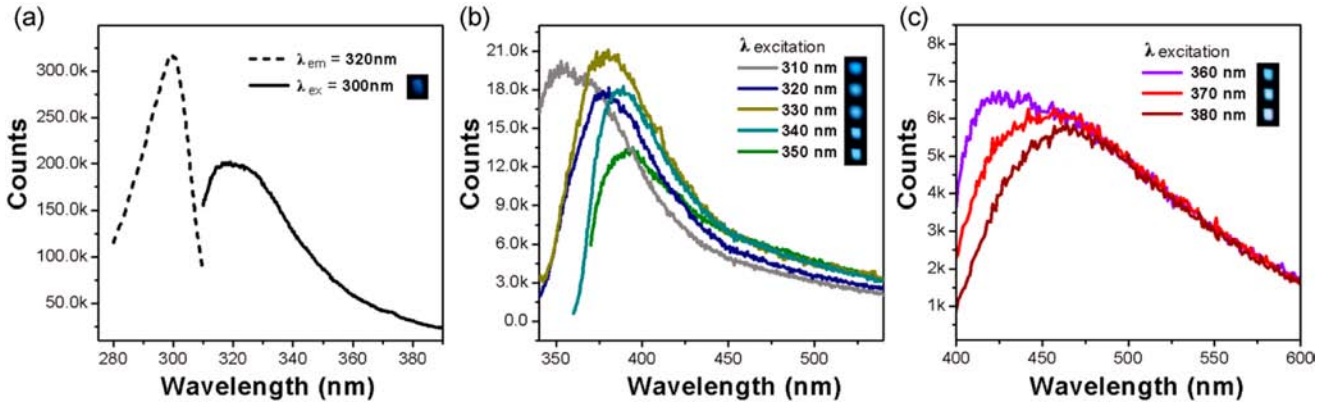

Figure 7. (a) Fluorescence curves of **1a** with the maximum emission at 320 nm upon 300 nm excitation. (b) Different emissions of **1a** by adjusting excitation wavelengths from 310 to 350 nm with a 10 nm step. (c) Different emissions of **1a** under excitations of 360, 370, and 380 nm, respectively. (Inset) Related fluorescence images.

dx.doi.org/10.1021/ic401409b | *Inorg. Chem.* 2013, 52, 10096−10104

wavelengths adjusted to >350 nm, the tetrazolate groups play a main role for the emission range of 430−470 nm, which can further be confirmed by excitation curves (Figure S11b, Supporting Information).[27] Temperature-dependent emission spectra of **1a** (Figure S12, Supporting Information) show that the luminescent intensity of the emission (320 nm) decreases gradually as the temperature increases from 100 to 300 °C because of the thermal activation through nonradiative decay pathways.[28]

Compound **2a** shows a strong blue luminescence emission peaked at 433 nm upon excitation at 367 nm (Figure 8). The

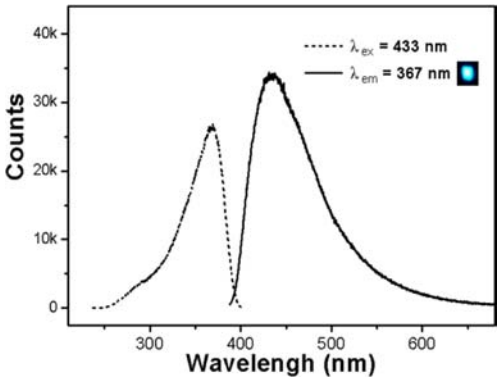

Figure 8. Solid-state excitation and emission spectra of **2a** at room temperature. (Inset) Related fluorescence image.

luminescence lifetime measurement shows that the value of the fluorescent lifetime is 0.80 ns (τ_1 = 0.22 ns, 87.46%; τ_2 = 4.87 ns, 12.54%; Figure S7, Supporting Information), which indicates that there may be one charge transfer transition. In light of the calculated DOS, the orbital edge of VBs and CBs in **2a** mainly originates from the tetrazolate contribution, without participation of the metal d electrons (Figure S13, Supporting Information). Therefore, the blue luminescence of **2a** is no doubt ascribed to a tetrazolate ligand-centered charge transition.[27]

Heat of Combustion. Tetrazoles and their derivatives have attracted considerable interest in applications as energetic materials and also display remarkable performance to meet the key requirements. Recently, metal energetic materials based on tetrazole derivatives have been obtained with high energy and low smoke character.[29] For nitrogen-rich **1a** and **2a**, which contain nitrogen contents of 23.11% and 21.31%, respectively, the constant-volume combustion heats (Δ_cU) were measured and the values are 20.903 and 14.160 kJ/g, respectively. The enthalpy of combustion (Δ_cH) was calculated from Δ_cU with a gas volume correction: $\Delta_cH = \Delta_cU + \Delta nRT$, where Δn depends on the charge about the number of gas constituents in reaction process. The calculated Δ_cH values of **1a** and **2a** are −20.903 and −14.158 kJ/g, respectively. The Δ_cH and relative parameters of classical explosives are listed in Table S4, Supporting Information. Obviously, compound **1a** possesses better energetic performance than traditional energetic materials, such as TNT with a Δ_cH value of −16.27 kJ/g. Compound **2a** also has larger Δ_cH than those of RDX and HMX but smaller than that of TNT. The high Δ_cH of **1a** and **2a** can be attributed to nitrogen-rich ligand and coordination effects resulting in close packing. The enthalpy of formation ($\Delta_fH°$) is an important characteristic of molecular structure, which mainly exists in chemical bonds of N−N, N−C, and C−C. The $\Delta_fH°$ values of **1a** and **2a** were calculated at 298.15 K using the Hess thermochemical cycle and combustion reactions as shown in eqs 1−4 and deduced as −256.41 and −1271.81 kJ/mol, respectively, with known enthalpies of ZnO (s, −348.00 kJ/mol), CO_2 (g, −393.51 kJ/mol), and H_2O (l, −285.83 kJ/mol). Compounds **1a** and **2a** should have thermodynamically stable structures with lower $\Delta_fH°$, which can be safely stored, compared with highly sensitive explosives. The tetrazolate-based CCs can serve as a new type of promising energetic material.

$$C_{14}H_{14}N_6O_2Zn(\mathbf{1a}, s) + 17O_2(g) \rightarrow ZnO(s) + 14CO_2(g) + 7H_2O(l) + 3N_2(g) \quad (1)$$

$$C_8H_{17}N_5O_5Zn(\mathbf{2a}, s) + 10.25O_2(g) \rightarrow ZnO(s) + 8CO_2(g) + 8.5H_2O(l) + 2.5N_2(g) \quad (2)$$

$$\Delta_fH°[\mathbf{1a}, s] = \Delta_fH°[ZnO, s] + 14\Delta_fH°[CO_2, g] + 7\Delta_fH°[H_2O, l] - \Delta_cH°[\mathbf{1a}, s] \quad (3)$$

$$\Delta_fH°[\mathbf{2a}, s] = \Delta_fH°[ZnO, s] + 8\Delta_fH°[CO_2, g] + 8.5\Delta_fH°[H_2O, l] - \Delta_cH°[\mathbf{2a}, s] \quad (4)$$

CONCLUSION

In this study, two pairs of new in-situ-generated chiral amino acid−tetrazole ligands (H_2tzet and H_2tzep) were employed to synthesize two pairs of enantiomorphs, homochiral Zn(II) coordination compounds **1** and **2**. Compound **1** exhibits a 2D framework formed by the linkage of Zn(II) atoms and $tzet^{2-}$ with high thermal stability (up to 380 °C), and **2** presents an isolated mononuclear structure accompanying a supramolecular 2D architecture resulting from the existence of plentiful hydrogen bonds. Homochiral configurations in **1** and **2** have been successfully realized by ligand chirality conservation and chirality induction and further confirmed by the results of experimental CD spectra, which fit well to the calculated ones. Theoretical investigation of CD spectra reveals that the chromophore of the indole group provides the main contributions for Cotton effects for **1**, and the stronger CD signal (~205 nm) of **2** comes from carboxylate n−π^* transitions and LMCT interactions (from the tetrazolate groups to Zn(II) atoms). Solid-state luminescent characteristics and the mechanism of **1** and **2** have been explored with the aid of a combination of experimental spectra and DOS theoretical calculations. Excitation wavelength-dependent (from 300 to 380 nm) emission spectra show that **1** possesses multiple emission centers and displays tunable UV-to-blue photoluminescence (from 320 to 470 nm). Examination of the combustion energy demonstrates that nitrogen-rich **1** and **2** possess comparable enthalpies of combustion (−20.90 and −14.16 kJ/g for **1** and **2**, respectively) with classical energetic materials (−16.27 kJ/g for TNT). Therefore, introduction of chiral amino acid in tetrazolate derivatives will be a good roadmap for design of homochiral coordination compounds or development of multifunctional materials.

ASSOCIATED CONTENT

Supporting Information

X-ray crystallographic data in CIF format, crystal structures, IR spectra, PXRD patterns, TG-DTA, theoretical CD parameters,

diffuse reflectance spectra, excitation and emission spectra, DOS calculation results, and thermochemical properties. This material is available free of charge via the Internet at http://pubs.acs.org.

AUTHOR INFORMATION

Corresponding Author

*E-mail: zfk@fjirsm.ac.cn.

Notes

The authors declare no competing financial interest.

ACKNOWLEDGMENTS

This work was financially supported by 973 Program (2011CBA00505) and the National Nature Science Foundation of China (20871115 and 21103188).

REFERENCES

(1) (a) Seo, J. S.; Whang, D.; Lee, H.; Jun, S. I.; Oh, J.; Jeon, Y. J.; Kim, K. *Nature* **2000**, *404*, 982−986. (b) Kitagawa, S.; Kitaura, R.; Noro, S. I. *Angew. Chem., Int. Ed.* **2004**, *43*, 2334−2375. (c) Shi, X.; Zhu, G.; Qiu, S.; Huang, K.; Yu, J.; Xu, R. *Angew. Chem., Int. Ed.* **2004**, *43*, 6482−6485. (d) Férey, G. *Chem. Soc. Rev.* **2008**, *37*, 191−214. (e) Liu, Y.; Xuan, W.; Cui, Y. *Adv. Mater.* **2010**, *22*, 4112−4135. (f) Wu, P. Y.; He, C.; Wang, J.; Peng, X. J.; Li, X. Z.; An, Y. L.; Duan, C. Y. *J. Am. Chem. Soc.* **2012**, *134*, 14991−14999. (g) Yoon, M.; Srirambalaji, R.; Kim, K. *Chem. Rev.* **2012**, *112*, 1196−1231. (h) Xuan, W. M.; Zhu, C. F.; Liu, Y.; Cui, Y. *Chem. Soc. Rev.* **2012**, *41*, 1677−1695.

(2) (a) Lin, W. B. *J. Solid State Chem.* **2005**, *178*, 2486−2490. (b) Zhang, J.; Yao, Y. G.; Bu, X. H. *Chem. Mater.* **2007**, *19*, 5083−5089. (c) Reger, D. L.; Horger, J. J.; Smith, M. D.; Long, G. J.; Grandjean, F. *Inorg. Chem.* **2011**, *50*, 686−704.

(3) (a) Lin, Z. J.; Slawin, A. Z.; Morris, R. E. *J. Am. Chem. Soc.* **2007**, *129*, 4880−4881. (b) Zhang, J.; Chen, S.; Wu, T.; Feng, P.; Bu, X. H. *J. Am. Chem. Soc.* **2008**, *130*, 12882−12883. (c) Morris, R. E.; Bu, X. H. *Nat. Chem.* **2010**, *2*, 353−361.

(4) (a) Gao, E. Q.; Yue, Y. F.; Bai, S. Q.; He, Z.; Yan, C. H. *J. Am. Chem. Soc.* **2004**, *126*, 1419−1429. (b) Yao, Q. X.; Xuan, W. M.; Zhang, H.; Tu, C. Y.; Zhang, J. *Chem. Commun.* **2009**, 59−61. (c) Chen, S.; Zhang, J.; Bu, X. H. *Inorg. Chem.* **2009**, *48*, 6356−6358. (d) Gil-Hernandez, B.; Höppe, H. A.; Vieth, J. K.; Sanchiz, J.; Janiak, C. *Chem. Commun.* **2010**, *46*, 8270−8272. (e) Tan, X.; Zhan, J. X.; Zhang, J. Y.; Jiang, L.; Pan, M.; Su, C. Y. *CrystEngComm* **2012**, *14*, 63−66.

(5) (a) Ingleson, M. J.; Bacsa, J.; Rosseinsky, M. J. *Chem. Commun.* **2007**, 3036−3038. (b) Crassous, J. *Chem. Soc. Rev.* **2009**, *38*, 830−845.

(6) (a) Anokhina, E. V.; Go, Y. B.; Lee, Y.; Vogt, T.; Jacobson, A. J. *J. Am. Chem. Soc.* **2006**, *128*, 9957−9962. (b) Wisser, B.; Lu, Y.; Janiak, C. *Z. Anorg. Allg. Chem.* **2007**, *633*, 1189−1192.

(7) (a) Sahoo, S. C.; Kundu, T.; Banerjee, R. *J. Am. Chem. Soc.* **2011**, *133*, 17950−17958. (b) Kundu, T.; Sahoo, S. C.; Banerjee, R. *Cryst. Growth Des.* **2012**, *12*, 4633−4640.

(8) (a) Xiong, R. G.; Xue, X.; Zhao, H.; You, X. Z.; Abrahams, B. F.; Xue, Z. *Angew. Chem., Int. Ed.* **2002**, *41*, 3800−3803. (b) Qu, Z. R.; Zhao, H.; Wang, X. S.; Li, Y. H.; Song, Y. M.; Liu, Y. J.; Ye, Q.; Xiong, R. G.; Abrahams, B. F.; Xue, Z. L.; You, X. Z. *Inorg. Chem.* **2003**, *42*, 7710−7712. (c) Ye, Q.; Song, Y. M.; Wang, G. X.; Chen, K.; Fu, D. W.; Chan, P. W. H.; Zhu, J. S.; Huang, S. P. D.; Xiong, R. G. *J. Am. Chem. Soc.* **2006**, *128*, 6554−6555.

(9) (a) Tao, Y.; Li, J. R.; Chang, Z.; Bu, X. H. *Cryst. Growth Des.* **2009**, *10*, 564−574. (b) Wu, M. F.; Wang, M. S.; Guo, S. P.; Zheng, F. K.; Chen, H. F.; Jiang, X. M.; Liu, G. N.; Guo, G. C.; Huang, J. S. *Cryst. Growth Des.* **2011**, *11*, 372−381.

(10) (a) Demko, Z. P.; Sharpless, K. B. *J. Org. Chem.* **2001**, *66*, 7945−7950. (b) Zhao, H.; Qu, Z. R.; Ye, H. Y.; Xiong, R. G. *Chem. Soc. Rev.* **2008**, *37*, 84−100. (c) Pachfule, P.; Das, R.; Poddar, P.; Banerjee, R. *Cryst. Growth Des.* **2010**, *10*, 2475−2478.

(11) Li, Y.; Xu, G.; Zou, W. Q.; Wang, M. S.; Zheng, F. K.; Wu, M. F.; Zeng, H. Y.; Guo, G. C.; Huang, J. S. *Inorg. Chem.* **2008**, *47*, 7945−7947.

(12) *CrystalClear, version 1.35; Software User's Guide for the Rigaku R-Axis, and Mercury and Jupiter CCD Automated X-ray Imaging System*; Rigaku Molecular Structure Corp.: Tokyo, Japan, 2002.

(13) *SHELXTL Reference Manual*, version 5; Siemens Energy & Automation Inc.: Madison, WI, 1994.

(14) (a) Segall, M.; Linda, P.; Probert, M.; Pickard, C.; Hasnip, P.; Clark, S.; Payne, M. *Materials Studio CASTEP*, version 2.2; Accelrys: San Diego, CA, 2002. (b) Segall, M.; Linda, P.; Probert, M.; Pickard, C.; Hasnip, P.; Clark, S.; Payne, M. *J. Phys.: Condens. Matter* **2002**, *14*, 2717−2744.

(15) (a) Wu, M. F.; Liu, Z. F.; Wang, S. H.; Chen, J.; Xu, G.; Zheng, F. K.; Guo, G. C.; Huang, J. S. *CrystEngComm* **2011**, *13*, 6386−6392. (b) Wu, M. F.; Xu, G.; Zheng, F. K.; Liu, Z. F.; Wang, S. H.; Guo, G. C.; Huang, J. S. *Inorg. Chem. Commun.* **2011**, *14*, 333−336.

(16) Addison, A. W.; Rao, T. N.; Reedijk, J.; van Rijn, J.; Verschoor, G. C. *J. Chem. Soc., Dalton Trans.* **1984**, 1349−1356.

(17) Janiak, C. *J. Chem. Soc., Dalton Trans.* **2000**, 3885−3896.

(18) Gillard, R. D.; Irving, H. M. *Chem. Rev.* **1965**, *65*, 603−616.

(19) Wang, S. H.; Zheng, F. K.; Wu, M. F.; Liu, Z. F.; Chen, J.; Guo, G. C.; Wu, A Q. *CrystEngComm* **2013**, *15*, 2616−2623.

(20) (a) Lifson, S.; Hagler, A. T.; Dauber, P. *J. Am. Chem. Soc.* **1979**, *101*, 5111−5121. (b) Wang, Y.; Yu, J.; Li, Y.; Shi, Z.; Xu, R. *Chem.—Eur. J.* **2003**, *9*, 5048−5055. (c) Matta, C. F.; Hernández-Trujillo, J.; Tang, T. H.; Bader, R. F. W. *Chem.—Eur. J.* **2003**, *9*, 1940−1951. (d) Johansson, A.; Håkansson, M. *Chem.—Eur. J.* **2005**, *11*, 5238−5248. (e) Ściebura, J.; Gawroński, J. *Chem.—Eur. J.* **2011**, *17*, 13138−13141.

(21) (a) Holzwarth, G.; Doty, P. *J. Am. Chem. Soc.* **1965**, *87*, 218−228. (b) Schellman, J. A. *Chem. Rev.* **1975**, *75*, 323−331. (c) Autschbach, J.; Jorge, F. E.; Ziegler, T. *Inorg. Chem.* **2003**, *42*, 2867−2877.

(22) Frisch, M. J.; Trucks, G. W.; Schlegel, H. B.; Scuseria, G. E.; Robb, M. A.; Cheeseman, J. R.; Scalmani, G.; Barone, V.; Mennucci, B.; Petersson, G. A.; Nakatsuji, H.; Caricato, M.; Li, X.; Hratchian, H. P.; Izmaylov, A. F.; Bloino, J.; Zheng, G.; Sonnenberg, J. L.; Hada, M.; Ehara, M.; Toyota, K.; Fukuda, R.; Hasegawa, J.; Ishida, M.; Nakajima, T.; Honda, Y.; Kitao, O.; Nakai, H.; Vreven, T.; Montgomery, J.;, Jr.; Peralta, J. E.; Ogliaro, F.; Bearpark, M.; Heyd, J. J.; Brothers, E.; Kudin, K. N.; Staroverov, V. N.; Kobayashi, R.; Normand, J.; Raghavachari, K.; Rendell, A.; Burant, J. C.; Iyengar, S. S.; Tomasi, J.; Cossi, M.; Rega, N.; Millam, N. J.; Klene, M.; Knox, J. E.; Cross, J. B.; Bakken, V.; Adamo, C.; Jaramillo, J.; Gomperts, R.; Stratmann, R. E.; Yazyev, O.; Austin, A. J.; Cammi, R.; Pomelli, C.; Ochterski, J. W.; Martin, R. L.; Morokuma, K.; Zakrzewski, V. G.; Voth, G. A.; Salvador, P.; Dannenberg, J. J.; Dapprich, S.; Daniels, A. D.; Farkas, Ö.; Foresman, J. B.; Ortiz, J. V.; Cioslowski, J.; Fox, D. J. *Gaussian 09*, Revision A.1; Gaussian, Inc.: Wallingford, CT, 2009.

(23) Bruhn, T.; Schaumlöffel, A.; Hemberger, Y.; Bringmann, G. *SpecDis*, version 1.53: University of Wuerzburg: Germany, 2012.

(24) Diedrich, C.; Grimme, S. *J. Phys. Chem. A* **2003**, *107*, 2524−2539.

(25) (a) Tong, X. L.; Hu, T. L.; Zhao, J. P.; Wang, Y. K.; Zhang, H.; Bu, X. H. *Chem. Commun.* **2010**, *46*, 8543−8545. (b) Worch, C.; Atodiresei, I.; Raabe, G.; Bolm, C. *Chem.—Eur. J.* **2010**, *16*, 677−683. (c) Wakai, A.; Fukasawa, H.; Yang, C.; Mori, T.; Inoue, Y. *J. Am. Chem. Soc.* **2012**, *134*, 4990−4997.

(26) (a) Dong, Z.; Zhao, L.; Liang, Z.; Chen, P.; Yan, Y.; Li, J.; Yu, J.; Xu, R. *Dalton Trans.* **2010**, *39*, 5439−5445. (b) Chen, F.; Wu, M. F.; Liu, G. N.; Wang, M. S.; Zheng, F. K.; Yang, C.; Xu, Z. N.; Liu, Z. F.; Guo, G. C.; Huang, J. S. *Eur. J. Inorg. Chem.* **2010**, 4982−4991.

(27) (a) Wu, M. F.; Zheng, F. K.; Wu, A Q.; Li, Y.; Wang, M. S.; Zhou, W. W.; Chen, F.; Guo, G. C.; Huang, J. S. *CrystEngComm* **2010**, *12*, 260−269. (b) Wang, S. H.; Zheng, F. K.; Wu, M. F.; Liu, Z. F.; Chen, J.; Guo, G. C.; Huang, J. S. *Inorg. Chem. Commun.* **2012**, *24*, 186−189.

(28) Furman, J. D.; Warner, A. Y.; Teat, S. J.; Mikhailovsky, A. A.; Cheetham, A. K. *Chem. Mater.* **2010**, *22*, 2255−2260.
(29) (a) Tao, G. H.; Twamley, B.; Shreeve, J. M. *Inorg. Chem.* **2009**, *48*, 9918−9923. (b) Gao, H.; Shreeve, J. M. *Chem. Rev.* **2011**, *111*, 7377−7436. (c) Tao, G. H.; Parrish, D. A.; Shreeve, J. M. *Inorg. Chem.* **2012**, *51*, 5305−5312.